10-15-2019

Pyrenylpyridines: Sky-Blue Emitters for Organic Light-Emitting Diodes

Thenahandi Prasanthi Deepthika De Silva
Louisiana State Univ, Dept Chem

Sang Gill Youm
Louisiana State Univ, Dept Chem

Isiah M. Warner
Louisiana State Univ, Dept Chem, iwarner@lsu.edu

ACS OMEGA

Article

Cite This: ACS Omega 2019, 4, 16867−16877

http://pubs.acs.org/journal/acsodf

Pyrenylpyridines: Sky-Blue Emitters for Organic Light-Emitting Diodes

Thenahandi Prasanthi Deepthika De Silva,[†] Sang Gil Youm,[†,§] George G. Tamas,[†,∥] Boqian Yang,[‡] Chun-Han Wang,[†,§] Frank R. Fronczek,[†] Girija Sahasrabudhe,[†,⊥] Sierra Sterling,[†] Rashanique D. Quarels,[†,#] Pratap K. Chhotaray,[†,¶] Evgueni E. Nesterov,[†,§] and Isiah M. Warner*[,†]

[†]Department of Chemistry, Louisiana State University, Baton Rouge, Louisiana 70803, United States

[‡]Horiba Scientific, 20 Knightsbridge Road, Piscataway, New Jersey 08854, United States

Supporting Information

ABSTRACT: A novel sky-blue-emitting tripyrenylpyridine derivative, 2,4,6-tri(1-pyrenyl)-pyridine (2,4,6-TPP), has been synthesized using a Suzuki coupling reaction and compared with three previously reported isomeric dipyrenylpyridine (DPP) analogues (2,4-di(1-pyrenyl)pyridine (2,4-DPP), 2,6-di(1-pyrenyl)pyridine (2,6-DPP), and 3,5-di(1-pyrenyl)-pyridine (3,5-DPP)). As revealed by single-crystal X-ray analysis and computational simulations, all compounds possess highly twisted conformations in the solid state with interpyrene torsional angles of 42.3°−57.2°. These solid-state conformations and packing variations of pyrenylpyridines could be correlated to observed variations in physical characteristics such as photo/thermal stability and spectral properties, but showed only marginal influence on electrochemical properties. The novel derivative, 2,4,6-TPP, exhibited the lowest degree of crystallinity as revealed by powder X-ray diffraction analysis and formed amorphous thin films as verified using grazing-incidence wide-angle X-ray scattering. This compound also showed high thermal/photo stability relative to its disubstituted analogues (DPPs). Thus, a nondoped organic light-emitting diode (OLED) prototype was fabricated using 2,4,6-TPP as the emissive layer, which displayed a sky-blue electroluminescence with Commission Internationale de L'Eclairage (CIE) coordinates of (0.18, 0.34). This OLED prototype achieved a maximum external quantum efficiency of 6.0 ± 1.2% at 5 V. The relatively high efficiency for this simple-architecture device reflects a good balance of electron and hole transporting ability of 2,4,6-TPP along with efficient exciton formation in this material and indicates its promise as an emitting material for design of blue OLED devices.

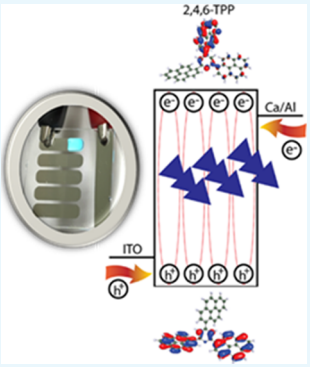

INTRODUCTION

Organic light-emitting diodes (OLEDs) occupy a significant niche in organic semiconductor-based technology, representing a promising means for next-generation electronic displays and solid-state lighting. Accordingly, an estimated global market share of $9.6 billion is expected by the year 2020 for OLEDs.[1] Perceived popularity of OLED displays over liquid-crystal displays is attributable to numerous cutting-edge advantages offered by OLEDs such as lower power consumption, self-emission, a greater color gamut, high resolution, high contrast, light weight, flexibility, transparency, and broader viewing angles.[1,2] Full color OLED displays often require emitters for the three primary colors of red, green, and blue. However, an intrinsically wide highest occupied molecular orbital (HOMO)−lowest unoccupied molecular orbital (LUMO) energy gap of blue emitters causes inefficient charge injection and rapid deterioration of the emissive layer upon excitation.[3,4] Consequently, blue emitters typically show inferior operational lifetime, efficiency, and color purity than red and green emitters.[1] Thus, limited availability of efficient, photothermally and chemically stable, spectrally pure, and highly processable organic blue emitters constitutes a major challenge for the progress of OLED technology. Unfortunately, this is a widespread problem among blue emitters with many variations in molecular designs including polymers, oligomers, dendrimers, organometallics, and small organic molecules.[4] Among these molecular designs, small-molecule organic blue emitters have some distinct advantages including ease of synthesis, purification, characterization, modification, and OLED fabrication.[3,4] A large fraction of these small-molecule organic blue emitters are derived from polyaromatic hydrocarbons (PAH) based luminophores such as anthracene, phenanthrene, fluorene, pyrene, carbazole, and indenopyrazine.[3−6] Among these luminophores, pyrene provides great potential for fabrication of OLEDs blue emitters owing to its high thermal and photo stabilities, favorable charge carrier properties, and spectral characteristics.[5,7] Consequently, a number of pyrene derivatives have already been reported as blue/green OLED emitters[7−12] as well as charge injectors/transporters in OLEDs.[7,13−18] More importantly, pyrene

Received: June 28, 2019
Accepted: September 25, 2019
Published: October 3, 2019

DOI: 10.1021/acsomega.9b01948
ACS Omega 2019, 4, 16867−16877

derivatives can be designed as multifunctional p-type, n-type, or bipolar emitters, ensuring an efficient and balanced flux of charges to the emissive layer even with relatively simple device architectures.[3,7]

A major challenge with many pyrene-based emissive materials is controlling undesirable excimer formation, particularly in the condensed state. The nearly planar aromatic conjugated ring system of pyrene readily undergoes $\pi-\pi$ stacking and consequent excimer formation. As a result, emission of most pyrene derivatives exhibits significant red shifts and often demonstrates aggregation-caused quenching, which affects color purity and device efficiency.[19−21] A notable exception for the aggregation-caused quenching of fluorescent dyes is an aggregation-induced emission (AIE) effect, which shows restriction of intramolecular rotation in the solid state, thus improving emission efficiency in the solid state.[22,23] Despite obvious advantages of AIE materials, they often contain chemically less stable aliphatic double bonds and/or heteroatomic functional groups.[22,23] Therefore, our research has focused on emitters based on chemically stable PAH ring systems, such as pyrenylpyridines discussed herein.

For non-AIE molecules that consist of multiple pyrene moieties, mutually twisting these intramolecular pyrene units is found to be effective for reducing dye aggregation in the solid state because of increased steric hindrance that prevents face-to-face pyrene aggregation.[17,20,24] For this reason, molecules with multiple pyrenyl moieties can be designed in such a way that the pyrene units are attached to rigid bridging molecular platforms, for example, benzene, calixarene, and octavinylsilsesquioxane.[17,20,24] These molecular designs provide sufficient steric strain to mutually twist the pyrene units into a nearly orthogonal conformation with respect to each other. These twisted conformations electronically isolate individual pyrene moieties within each molecule to minimize extended conjugation, as well as reduce solid-state intermolecular $\pi-\pi$ stacking as a result of steric hindrance.[17,20,24] Accordingly, such molecular designs confine the luminophore emission largely within the blue region of electromagnetic spectrum (EMS), while minimizing aggregation-caused quenching.[17]

In the study reported herein, four pyrenylpyridines were used as model compounds to evaluate the structure−property relationships in pyrene-containing small organic molecules. Among these pyrenylpyridines, 2,4-di(1-pyrenyl)pyridine (2,4-DPP), 2,6-di(1-pyrenyl)pyridine (2,6-DPP), and 3,5-di(1-pyrenyl)pyridine (3,5-DPP), each possessing two pyrene units, are thus collectively referred to as dipyrenylpyridines (DPPs), whereas 2,4,6-tri(1-pyrenyl)pyridine (2,4,6-TPP) has three pyrene units. In addition, molecular symmetry of these structural isomers shows much diversity with 2,4-DPP being asymmetric, while 2,6-DPP, 3,5-DPP, and 2,4,6-TPP each display a formal plane of symmetry. The pyridine unit is used as a bridging moiety to induce enough steric strain to intramolecularly twist the pyrenyl moieties for control of dye aggregation.

During the course of this study, it was noted that despite the significantly twisted conformations of pyrenylpyridines, $\pi-\pi$ stacking occurs in the solid state to varying degrees, depending on a multitude of factors such as molecular symmetry, solid-state conformation, and the extent of inter- and intramolecular interactions between pyrene units. As a result, solid-state characteristics of pyrenylpyridines, including absorption and photoluminescence spectra, fluorescence lifetimes, photoluminescence quantum yields (PLQYs), melting points, thermal decomposition onset temperatures, and the degree of crystallinity, were found to be significantly different among these compounds, despite their structural similarities.

It is noted that the DPP compounds, 3,5-DPP and 2,6-DPP, have been previously reported as electron-transporting materials, and 2,4-DPP has been previously mentioned in a few patents.[13,25,26] However, to the best of our knowledge, these compounds have not been evaluated for suitability as blue OLED-emissive materials. Furthermore, 2,4,6-TPP is a novel compound that has not been described in literature. This compound exhibits the most favorable characteristics for blue OLED emission, including highest quantum yield, thermal and photo stabilities, and the lowest degree of crystallinity, among the pyrenylpyridines investigated. Accordingly, a nondoped, bottom-emitting OLED prototype based on 2,4,6-TPP as the emissive layer was fabricated. This device showed sky-blue electroluminescence with maximum EQE of 6 (±1.2)% at 5 V. It is noteworthy that the theoretical upper limit of external quantum efficiency (EQE) for a typical bottom emitting OLED utilizing conventional fluorescence as the exciton harvesting mechanism is estimated as 5%.[4,6] This estimation is based on the fact that only 25% of all excitons formed under electroluminescent conditions are formed in singlet state, and thus are available to be harvested by conventional fluorescence. In addition, the light outcoupling efficiency of a typical bottom emitting OLED is approximated as only 20%.[4,6] Accordingly, the EQE value obtained for the OLED prototype described herein is comparable to the best OLEDs based on conventional architectures with small-molecule fluorescent emitters.

RESULTS AND DISCUSSION

Solid-State Packing and Thin Film Morphology. Solid-state conformation often influences molecular aggregation and thin-film morphology, thus affecting photo-physical properties of chromophoric compounds, particularly in the condensed state. Therefore, molecular conformations of the pyrenylpyridines were elucidated using powder X-ray diffraction (PXRD) and single-crystal XRD techniques and presented in Figures S1−S3 in the Supporting Information. As revealed by PXRD, 2,4,6-TPP is an amorphous material, whereas all three DPPs are crystalline solids (see Figure S2 in the Supporting Information).

The observed degree of crystallinity variations of pyrenylpyridines can be correlated to the conformational changes in these compounds. For example, much bulkier 2,4,6-TPP may reduce the packing efficiency in the solid-state than symmetric 2,6-DPP and 3,5-DPP and asymmetric, but less bulkier 2,4-DPP. With the exception of 2,4,6-TPP, all pyrenylpyridines formed high-quality single crystals suitable for single-crystal XRD structure determination. Crystal structures of three DPP compounds are available in crystallographic information file formats, CCDC 1560016 (2,4-DPP), CCDC 1560018 (2,6-DPP), and CCDC 1560019 (3,5-DPP). Intermolecular distances and torsion angles of the DPPs derived from single-crystal XRD experiments are listed in Table 1. According to single-crystal XRD data, all three DPP compounds adopt significantly twisted conformations in the solid-state, with torsion angles between pyrenyl and pyridine moieties ranging from 42 (12)° to 47 (18)°, suggesting that intramolecular twisting is significant and occurs more or less to the same extent in all DPPs. Computed torsion angle values for DPPs were very close to the experimental values as shown in Table 1. The computed average torsion angle in 2,4,6-TPP was 49.58

DOI: 10.1021/acsomega.9b01948
ACS Omega 2019, 4, 16867−16877

Table 1. Summary of Conformational and Thermal Properties of Pyrenylpyridines

compound	T_m (°C)	T_g (°C)	T_{onset} (°C)	intermolecular distance (Å)	torsion angle (deg)[c]
2,4-DPP	172	99	361	6.86(3)[a]	47.48(18)[d]
				6.86(3)[b]	52.28(6)[e]
2,6-DPP	273	96	387	4.72(5)[a]	42.33(12)[d]
				5.16(11)[b]	43.75(2)[e]
3,5-DPP	281	106	387	3.40(3)[a]	46.74(18)[d]
				3.90(3)[b]	57.21(1)[e]
2,4,6-TPP	312	70	471	N/A	49.58(7)[e]

T_m: melting point, T_g: glass transition temperature, T_{onset}: decomposition onset temperature, closest C−C distance. [a]And N−N distance. [b]Between two neighboring pyrenylpyridine molecules in the single crystal, angle between pyrenyl and pyridine units of pyrenylpyridines. [c]Experimental torsion angles obtained from single-crystal XRD. [d]Torsion angles obtained from DFT computations.[e] N/A: Not available.

(7)°, confirming a twisted geometry similar to the DPPs. However, the addition of a third pyrenyl moiety in 2,4,6-TPP had virtually no effect on the extent of intramolecular twisting of the pyrene moieties, since positioning of three pyrene units around the pyridine moiety in 2,4,6-TPP provided comparable steric effects to intermolecular pyrene units as in DPPs. Despite this significant intramolecular twisting of pyrenyl units, the DPPs managed to arrange in an apparent zig-zag order (Figure S3 in the Supporting Information), allowing the pyrenyl moieties to undergo significant $\pi-\pi$ stacking. The intermolecular distances measured using C−C distances and N−N distances of neighboring DPP molecules in crystals ranged from 6.86 (±3) to 3.63 (±5) Å (for C−C) and 6.86 (±3) to 3.86 (±7) Å (for N−N), as a result of differences in solid-state packing induced by the combination of factors such as the extent of intramolecular twisting, inter- and intramolecular interactions, and molecular symmetry. Based on intermolecular distances, solid-state packing efficiencies of DPPs increased in the following order: 2,4-DPP < 2,6-DPP < 3,5-DPP.

Grazing-incidence wide-angle X-ray scattering (GIWAXS) is a useful technique to study the morphology and structural features in organic thin films and provides more realistic morphological information in thin films than PXRD and single-crystal XRD techniques.[36] Accordingly, GIWAXS studies on vacuum-deposited thin films of 2,4,6-TPP revealed that there were no distinct diffraction features arising from crystalline condensed matter (Figure 1), as noted by the appearance of an amorphous broad scattering at q = 1.51 Å. This pattern indicated that 2,4,6-TPP thin films were essentially amorphous, with no preferred crystalline packing of TPP molecules. Amorphous properties are particularly suitable for materials to be used in thin film electroluminescent devices because crystallinity may undesirably influence thermal stability, reproducibility of device parameters, and such solid-state characteristics as conductivity and photothermal reactivity.[37]

Computational Studies. Density functional theory (DFT) computational studies were performed to confirm structural and electrochemical characteristics of the pyrenylpyridines. All optimized geometries showed twisted structures with torsion angles between pyrenyl and pyridine units, within each molecule, comparable to experimental torsion angles obtained using single-crystal XRD (Table 1). In addition, details of frontier molecular orbitals were computationally

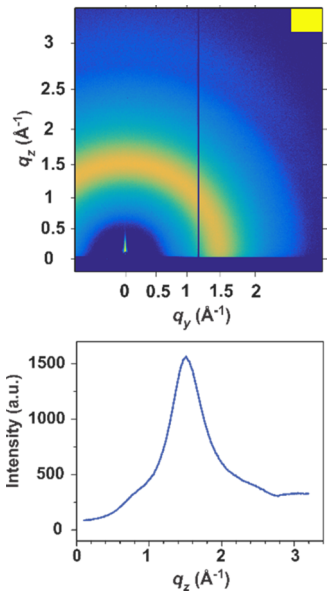

Figure 1. Two-dimensional GIWAXS image of a 2,4,6-TPP thin film on a quartz substrate (top) and vertical linecut of the GIWAXS data (bottom).

obtained for all pyrenylpyridines. Noticeably, HOMO of 2,4,6-TPP was distributed over two pyrenyl components while LUMO was primarily located on the third, orthogonal pyrenyl moiety (Figure 2). The asymmetric 2,4-DPP also showed

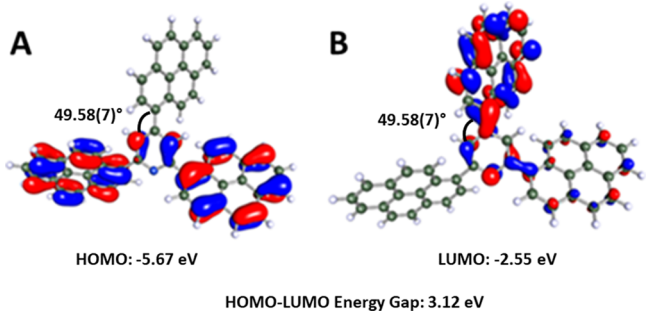

Figure 2. HOMO (A) and LUMO (B) of 2,4,6-TPP.

disjoint, spatially separated frontier molecular orbitals (Figure S4 in Supporting Information). In contrast, symmetric molecules 2,6-DPP and 3,5-DPP displayed more "congruent" frontier molecular orbitals distributed over the same pyrenyl fragments (Figure S4 in the Supporting Information). The disjoint, spatially localized on different pyrenyl fragments nature of the frontier molecular orbitals of 2,4,6-TPP (and also 2,4-DP) could contribute to a more balanced electron and hole transport in this material, which could benefit design of electroluminescent devices. HOMO−LUMO energy gaps obtained using computational studies were slightly higher (approximately 0.1−0.4 eV) than values obtained using low-energy onsets of the absorption bands of compounds in UV−vis absorption spectroscopy (Table S1 in the Supporting Information). This difference may be the result of the computational studies being done in the gas phase, whereas experimental determinations were performed on condensed phases of these compounds.

Thermal and Photo Stabilities of Pyrenylpyridines. Resistance to thermal degradation is crucial for longevity of

DOI: 10.1021/acsomega.9b01948
ACS Omega 2019, 4, 16867−16877

OLED devices.[38,39] In this regard, thermal stabilities of pyrenylpyridines were evaluated using thermogravimetric analysis (TGA).[40] The resultant TGA profiles of pyrenylpyridines are shown in Figure S5 in the Supporting Information, and T_{onset} values are listed in Table 1. Interestingly, all compounds exhibited high thermal stabilities with T_{onset} values in the range of 361−471 °C. It is noted that the T_{onset} values of DPPs were distributed over a narrow range of 361−387 °C. The significantly higher thermal stability of 2,4,6-TPP with T_{onset} value of 471 °C, which is 18−23% higher than that of typical DPPs, is attributed to higher molecular weight of this compound, with an extra pyrenyl unit resulting in increased magnitude of combined van der Waals intermolecular interactions between 2,4,6-TPP molecules in the solid-state. As revealed using PXRD, 2,4,6-TPP is the only amorphous material investigated, but has the highest T_{onset} and T_g values.

All pyrenylpyridines were high-melting solids, with melting points (T_m) ranging from 172 to 312 °C. Melting temperatures of pyrenylpyridines increased in the following order: 2,4-DPP < 2,6-DPP < 3,5-DPP < 2,4,6-TPP, which paralleled the trend in the solid-state packing efficiency. For example, 2,4-DPP had the lowest packing efficiency (as discussed in the XRD section), and also showed the lowest T_m (172 °C). The glass transition temperature (T_g) is defined as the temperature at which a hard material is transformed to a more pliable state.[41] Therefore, exceeding the temperature of a thin organic emissive film in an OLED device above T_g may significantly affect device performance because temperature-induced defects caused by several phenomena including phase separation, crystallization, dewetting and mixing may occur above T_g.[41] On the other hand, lower T_g indicates that in normal conditions, the material remains more flexible and pliable, and less susceptible to mechanical stress and deformation induced degradation. Therefore, T_g values for all pyrenylpyridines were determined using differential scanning calorimetry (see Figure S6 in Supporting Information and Table 1 for T_g values summary). It is noted that DPPs had higher T_g values (in the range of 96−106 °C) than 2,4,6-TPP (70 °C). Thus, thermal stability of the pyrenylpyridines could be directly correlated to factors such as molecular symmetry, solid-state conformation, and the extent of intermolecular interactions.

Among various degradation processes of organic semiconductors that ultimately lead to device malfunction, photodegradation is one possible pathway.[42,43] Although the exact mechanisms involved in these light-induced reversible/irreversible oxidation processes may vary for a given molecule and are not always fully understood, it has been suggested that radical dark states may be involved in these photobleaching mechanisms.[43,44] Photostability of pyrenylpyridines was evaluated using a previously reported procedure developed for organic dyes.[45,46] In a typical time-dependent kinetic photostability experiment, the compound is intensively irradiated using monochromatic light of the wavelength set at the absorption maximum for a sufficient time period, while recording the photoluminescence intensity fluctuations at the respective emission maximum of the compound. Because of photodegradation, photolabile compounds typically show an exponential decrease in emission intensity when intensively irradiated.[46] Therefore, it is assumed that this decay of emission intensity observed with increased irradiation time is proportional to the extent of photobleaching. Accordingly, photostability of pyrenylpyridines was determined using eq 1.

$$\text{Photostability (\%)} = \left(\frac{I}{I_0}\right) \times 100\% \quad (1)$$

where I is the emission intensity after intensive irradiation and I_0 is the observed emission intensity before irradiation. Resultant time-dependent photoluminescence intensity fluctuation curves of all pyrenylpyridines are presented in Figure S7 in the Supporting Information. It is noted that all pyrenylpyridines maintained stable photoluminescence, that is there was no measurable photobleaching upon intense irradiation under the given experimental conditions and time period. These photobleaching curves of pyrenylpyridines are similar to those of other photostable compounds evaluated using time-dependent kinetic photostability experiments.[47] The enhanced photostability exhibited by pyrenylpyridines could be attributed to pyrenyl moieties that are highly resistant to photodegradation under ambient conditions.

Spectral Properties in Solution and Solid State. UV−vis absorption spectra of pyrenylpyridines were recorded in dilute chloroform solution (5 μM) and in thin solid films. Thin solid films of pyrenylpyridines were formed on quartz slides using electro-spray deposition (1 mM in DCM, flow rate 100 μL min^{-1}, applied voltage 2.8 V, and applied current 3 A). The absorption spectra obtained for solution and solid films of pyrenylpyridines are presented in Figure 3 and values of absorption maxima and full widths at half maxima (fwhm) are summarized in Table 2.

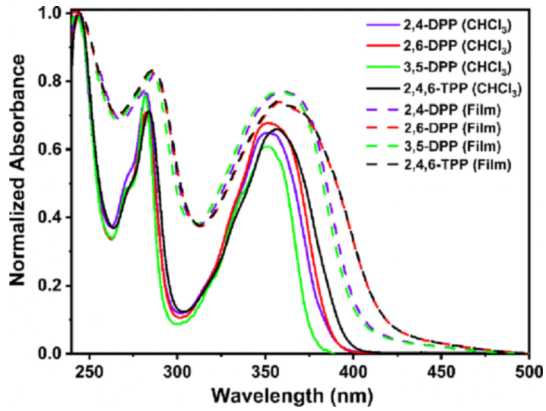

Figure 3. Normalized absorption spectra of pyrenylpyridines in dilute chloroform solution and as thin films on quartz substrate.

Accordingly, all pyrenylpyridines showed three broad absorption bands in both solution and solid state, with absorption peak maxima (A_{max}) at 244 ± 1 nm (A_{max3}), 282 ± 2 nm (A_{max2}), and 353 ± 3 nm (A_{max1}). Solution and solid-state absorption spectra largely resembled those of pyrene as a result of the high pyrenyl fraction (84% for 89% for DPPs and 2,4,6-TPP by weight) of these compounds. Accordingly, absorption peaks are assigned to S_0 to S_3 (A_{max3}), S_0 to S_2 (A_{max2}), and S_0 to S_1 (A_{max1}) electronic transitions.[21,48] There was substantial broadening of the absorption bands due to interchromophore electronic interactions. Such interactions could happen between pyrenyl groups in the same molecule, which was confirmed by the delocalization of molecular orbitals found in computational studies (vide supra). Further broadening could be attributed to intermolecular electronic interactions in the condensed phase (solid state). Accordingly, for solid-state absorption spectra, absorption peaks of pyrenylpyridines were

DOI: 10.1021/acsomega.9b01948
ACS Omega 2019, 4, 16867−16877

Table 2. Absorption Spectroscopy Data for Pyrenylpyridines

compound	absorption maxima (nm)		fwhm (nm)	
	sol.[a]	film	sol.[a]	film
2,4-DPP	244	241	19	56
	282	286	25	59
	353	358	46	75
2,6-DPP	245	240	20	64
	282	287	25	37
	352	355	48	74
3,5-DPP	244	243	20	61
	282	286	21	41
	351	358	41	83
2,4,6-TPP	244	244	19	58
	284	286	27	37
	356	361	51	69

[a]In chloroform (5 μM).

significantly broadened with average fwhm values of 77 nm (A_{max1}), 43 nm (A_{max2}), and 58 nm (A_{max3}) larger in solid films than in solution (48 nm for A_{max1}, 24 nm for A_{max2}, and 19 nm for A_{max3}, respectively) and red-shifted (≤7 nm).

Photoluminescence spectra of all pyrenylpyridines were recorded in dilute chloroform solutions (1 μM) and in thin solid films prepared by electro-spray deposition as described in the previous section. Photoluminescence spectra of pyrenylpyridines are presented in Figure 4. Also, emission maxima and

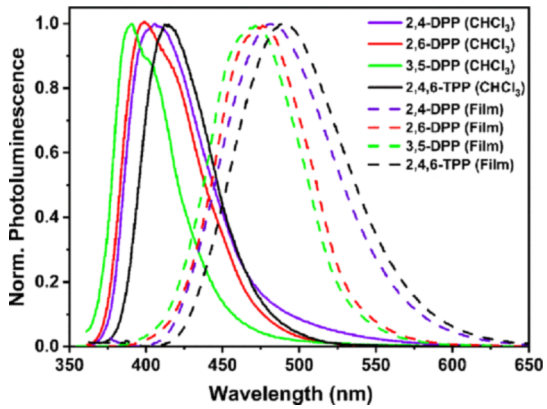

Figure 4. Normalized emission spectra of pyrenylpyridines in dilute chloroform solutions and as thin films on quartz substrate.

fwhm values are summarized in Table 3. Emission spectra of all pyrenylpyridines in dilute solution were largely resembling pyrene emission (emission maxima in the range of 392−440 nm), albeit the single band was substantially broadened and showed no fine vibronic structure.[48] In thin solid films, the pyrenylpyridines showed a substantially bathochromically shifted emission band (emission maximum in the range of 463−494 nm) with significant broadening (as denoted by the increase of fwhm values approximately by 20−30 nm). A bathochromic shift and broadening of the emission bands are characteristic to pyrene excimer formation.[12,48] The required presence of close cofacial contacts between pyrenyl units of the adjacent molecules was found in the single-crystal X-ray structures of DPPs (vide supra). Because emission in the solid-state is controlled by excitation transfer to the lowest energy chromophores (which would, in this case, be cofacially arranged pyrene units), all pyrenylpyridines studies in this work showed very similar solid-state emission spectra. However, dye aggregation was not as extensive as reported in many cases for pyrene derivatives, where both photo- and electro-luminescence (in terms of quantum efficiencies) are significantly reduced as a result of aggregation-induced quenching.[7,49,50]

Photoluminescence of pyrenylpyridines was approximately confined to the violet-blue region of the EMS in dilute solutions and greenish-blue region of the EMS in the solid-state. The colors of these compounds were assigned using CIE coordinates (Table 3) and all appeared in the range of (0.162 ± 0.003, 0.040 ± 0.016) for solutions and (0.149 ± 0.018, 0.235 ± 0.090) for solid-state. Because the pyrenylpyridine compounds incorporate both the electron donating (pyrene) and electron accepting (pyridine) moieties in the same molecule, this potentially could lead to the formation of intramolecular charge transfer (ICT) states. Formation of ICT states could, in principle, lead to undesirable changes in spectral characteristics including bathochromic shifts, broadening of the spectral bands, and decreasing fluorescence quantum efficiency. In order to check for possible formation of ICT states, we studied solvatochromic behavior of the pyrenylpyridines. Photoluminescence spectra of these compounds were recorded in hexane, methanol, and dimethyl sulfoxide (DMSO) solvents with polarity indices in the range of 0−7.2 (Figure S8 and Table S2 in the Supporting Information). The emission band maxima of all four compounds slightly red-shifted with increasing solvent polarity from 394 ± 2 nm (hexane) to 435 ± 10 nm (DMSO), suggesting the possibility of some charge transfer participation in photoluminescence spectra.

However, possible contribution of ICT states was likely negligible as could be discerned from nearly identical absorption and emission excitation spectra (an example of absorption, excitation, and emission spectra of 2,4,6-TPP in chloroform solution (5 μM) is presented in Figure 5). The absorption and emission spectra obey "the mirror image rule", suggesting no major geometrical changes in the excited state.[21]

Table 3. Summary of Emission Properties of Pyrenylpyridines

compound	emission maxima (nm)		fwhm (nm)		Stokes shift (nm)		CIE coordinates (x,y)		PLQY (%)		lifetime (ns)
	sol.[a]	film	sol.[a]	film	sol.[a]	film	sol.[a]	film	sol.[a]	film	
2,4-DPP	406	463	59	82	53	107	0.162, 0.062	0.159, 0.279	79	47	7.66
2,6-DPP	400	468	55	77	48	116	0.159, 0.027	0.135, 0.144	74	51	6.28
3,5-DPP	392	476	44	69	41	125	0.165, 0.037	0.132, 0.175	76	55	6.12
2,4,6-TPP	412	494	52	85	56	141	0.160, 0.029	0.170, 0.343	89	64	4.25

[a]In chloroform (1 μM).

DOI: 10.1021/acsomega.9b01948
ACS Omega 2019, 4, 16867−16877

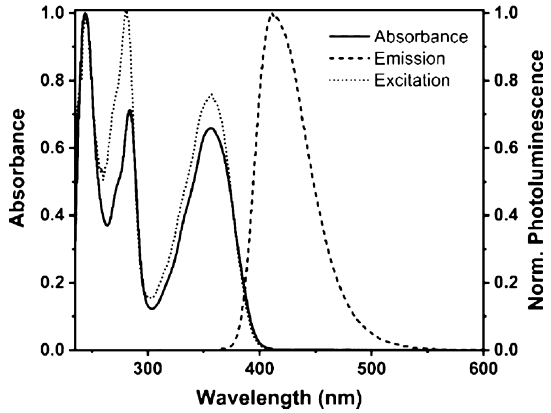

Figure 5. Normalized absorbance and excitation and emission spectra of 2,4,6-TPP in chloroform solution.

High photoluminescence efficiency is an important prerequisite for good OLED emitters, but is not the only criterion for determining electroluminescence efficiency of OLED emitters. This is because the electroluminescence mechanism of an emitter may be influenced by additional factors that are independent on photoluminescence mechanism, for example, electroluminescence efficiency is strongly affected by OLED architecture and material's electrical properties.[49,50] Photoluminescence efficiency of an OLED emitter is determined in terms of PLQY, defined as the ratio of emitted photons to absorbed photons.[21] For this reason, absolute quantum yields of pyrenylpyridines in dilute chloroform solutions and in thin films were determined using an integrating sphere attachment to a spectrofluorometer.[51] Table 3 summarizes the PLQY values measured for pyrenylpyridines. As shown, 2,4,6-TPP displayed the highest quantum yield in solution (89%) as well as in thin film (64%). The increased photoluminescence efficiency was likely due to decreased interactions between pyrenyl units in 2,4,6-TPP owing to its more sterically hindered geometry. In addition, completely amorphous thin-film morphology of 2,4,6-TPP could also contribute to the increased PLQY. The DPPs showed PLQY values in the range of 74−79% in solution and 47−55% in solid films. Accordingly, and despite noticeable aggregation in the solid-state, substantial PLQY values were observed for all pyrenylpyridines.

Fluorescence lifetime measurements were performed for each of the pyrenylpyridine compounds. Table 3 and Figure S9 in the Supporting Information provide summaries of lifetime data and decay curves for these compounds in solid-films. Fluorescence decay curves of all four compounds showed single-exponential decays indicating a single pathway for energy relaxation of photoluminescence from the singlet excited state in all cases.[21] The fluorescence lifetimes of pyrenylpyridines were distributed in the range of 7.66−4.25 ns. Fluorescence lifetimes of pyrenylpyridines increased in the following order: 2,4-DPP < 2,6-DPP < 3,5-DPP < 2,4,6-TPP, which is opposite to the trend in the solid-state obtained from single-crystal XRD (except for 2,4,6-TPP, which lacks single crystal XRD data due to amorphous nature). Because the extent of inter-molecular interactions (which is correlated to packing efficiency) plays a key role in determining lifetimes of fluorophores,[48] the trend of lifetimes observed for DPPs can easily be explained. For example, 2,4-DPP has the lowest packing efficiency and therefore the lowest intermolecular interactions and lowest nonradiative deexcitation. Thus, the highest fluorescence lifetime is observed for 2,4-DPP. For 2,4,6-TPP. However, the exact reasons for the observed lowest fluorescence lifetime are not clear. It is noted that 2,4,6-TPP has the lowest HOMO−LUMO energy gap, which could make nonradiative deexcitation relatively facile for 2,4,6-TPP than for DPPs and the presence of an additional pyrenyl unit may aid in additional intermolecular interactions that could contribute to the observed lowest lifetime.

Electronic Characteristics. Estimating HOMO and LUMO energies and HOMO−LUMO energy gaps (E_g) of OLED emitters is crucial for designing OLED devices.[52] Typically, semiconducting materials display energy gaps in the range of 0−4 eV.[52] The E_g values of all pyrenylpyridines were experimentally determined using UV−vis absorption spectra; in particular, λ_{edge} values indicate the minimum energy required to promote an electron from the ground state to the first excited state and are related to E_g (eq 3).[45] Alternatively, energies of frontier molecular orbitals and E_g could be evaluated using cyclic voltammetry (CV). Experimental spectroscopic E_g values were in the range of 3.10−3.28 eV as shown in Table 4. HOMO energies of pyrenylpyridines

Table 4. Electronic Properties of Pyrenylpyridines

compound	E_g (eV)	HOMO (eV)	LUMO (eV)
2,4-DPP	3.15	−5.75	−2.60
2,6-DPP	3.16	−5.76	−2.60
3,5-DPP	3.28	−5.70	−2.42
2,4,6-TPP	3.12	−5.67	−2.55

were experimentally obtained using CV by employing eq 2.[52,54] All pyrenylpyridines displayed quasi-reversible cyclic voltammograms with measurable oxidation peaks (Figure S10 in the Supporting Information). Quasi-reversible behavior is often displayed by redox couples when one state (oxidation or reduction) is not stable on the time scale of the CV experiment.[55] Accordingly, LUMO values were calculated using eq 3 using E_g values from UV−vis spectroscopy.[45,46] In eq 2, E_{ox} is the onset potential value of the oxidation peak obtained from cyclic voltammograms. The energy values experimentally determined for frontier molecular orbitals of the pyrenylpyridines were in the respective ranges of −5.67 to −5.76, and −2.42 to −2.60 eV (Table 4).[53]

$$\text{HOMO (eV)} = -1e[E_{ox.} + 4.71]\ \text{eV} \quad (2)$$

$$E_g\ \text{(eV)} = [\text{HOMOeLUMO}] = \frac{hc}{\lambda_{edge}} = \frac{1240}{\lambda_{edge}}\ \text{eV} \quad (3)$$

Characterization of OLED Prototype Fabricated Using 2,4,6-TPP as the Emissive Layer. OLED emitters in emissive layers (EMLs) can be embedded into an energetically matching host matrix (doped) or used as is, without such matrices (nondoped/self-host).[3,4] Doped EMLs have distinct advantages such as reduction in aggregation-caused quenching and the possibility to benefit from a favorable energy transfer between host matrix and emitter, which typically improve device performance.[3,4] Disadvantages associated with doping, however, include (1) phase separation-induced degradation, (2) limited availability of energetically matching host materials for blue emitters, and (3) complexity in device fabrication.[3,4] Considering pros and cons of doped EMLs, for preliminary studies presented herein, a nondoped

DOI: 10.1021/acsomega.9b01948
ACS Omega 2019, 4, 16867−16877

OLED prototype was fabricated to reduce complexity of device fabrication and to understand electroluminescent properties of a pure emitter. Because 2,4,6-TPP displayed the most promising photophysical characteristics among the pyrenylpyridines under study (i.e., highest PLQY in solid state, highest thermal stability, and lowest degree of crystallinity), an OLED prototype was fabricated using 2,4,6-TPP as the nondoped emissive layer. These prototypes were fabricated using a vacuum thermal evaporation (VTE) method, in accordance with state-of-the-art fabrication.[29] Fluorescence microscopy imaging was used to characterize 2,4,6-TPP films (Figure S11 in Supporting Information). The configuration of the OLED prototype was as follows: ITO (140 nm)/NPB (35 nm)/2,4,6-TPP (35 nm)/TPBI (30 nm)/Ca (12 nm)/Al (100 nm) as schematically shown in Figure 6A (NPB is *N*,*N*′-di(1-naphthyl)-*N*,*N*′-diphenyl-(1,1′-biphenyl)-4,4′-diamine, and TPBI is 1,3,5-tris(1-phenyl-1*H*-benzimidazole-2-yl)benzene). In this OLED prototype, NPB and TPBI were hole transport and electron transport layers, respectively, and 2,4,6-TPP was used as the nondoped emissive layer, whereas ITO was employed as the anode and Ca as the cathode (the schematics of OLED prototype and energy diagram are shown in Figure 6A,B). Device performance metrics were obtained in accordance with previously reported standard protocols.[6,56] Interestingly, a sky-blue electroluminescence was observed from this OLED prototype with a turn-on voltage of 4 V as shown in Figure 7A. The electroluminescence spectrum of this device was analogous to the observed photoluminescence from a thin film of 2,4,6-TPP, with peak maximum at 490 nm (Figure S12 in Supporting Information). Thus, the electroluminescence mechanism of the 2,4,6-TPP emissive layer is assumed to be based on conventional fluorescence.[4] The device reached maximum EQE of 6.0 (±1.2)% at 5 V with luminance of 36.2 (±4.7) cd m^{-2}, power efficiency of 8.0 (±1.9) Lm W^{-1}, and current efficiency of 6.3 (±1.5) cd A^{-1}. This device showed much brighter electroluminescence upon gradual increasing voltage, with luminance reaching 100 cd m^{-2} at 7.5 V. At this luminance, an EQE of 1.2 (±0.1)%, power efficiency of 1.1 (±0.1) Lm W^{-1}, and current efficiency of 1.4 (±0.1) cd A^{-1} were measured. The overall prototype performance is graphically presented in Figure 7B.

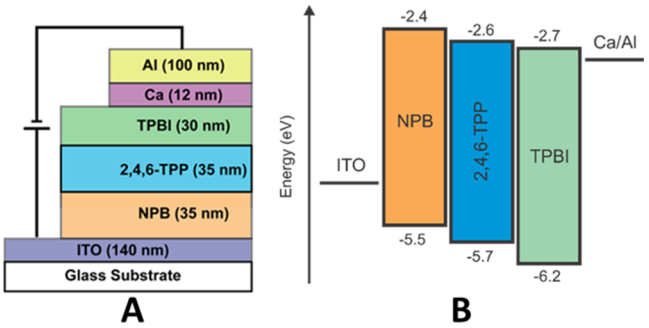

Figure 6. Device architecture (A) and energy diagram (B) for OLED prototype using 2,4,6-TPP as the emissive layer. (Please note that the architecture of this OLED device is not drawn proportionally).

The CIE coordinates for electroluminescence of the prototype device were (0.154, 0.297). The CIE spectral coordinate criterion for a blue emitter in an electronic display with RGB sub-pixel design is (y < 0.150, (x + y) < 0.300).[3] However, the National Television System Committee (NTSC) and European Broadcast Union (EBU) require much more spectrally pure blue emitters for RGB sub-pixel design based electronic displays, particularly television screens, with CIE coordinates of (0.140, 0.080) and (0.150,0.060), respectively.[4] Interestingly, light blue emitters are indispensable in non-conventional electronic displays. For example, a sub-pixel design known as red-green-light blue-deep blue (RGB_1B_2) that was invented by Universal Display Corporation (USA) contains a light blue component to generate colors that do not essentially require deep blue.[57,58] Such novel RGB_1B_2 sub-pixel designs promise advantages including significant power saving, improved device lifespan, and minimum emission of a harmful near-UV radiation.[58−60] Therefore, the sky-blue OLED emitter described here may be successfully applied in novel pixel designs that contain a light blue component.[59,60]

CONCLUSIONS

A series of structurally similar pyrenylpyridine compounds was successfully synthesized and spectral, physical, and electrical properties of these compounds were thoroughly investigated. Although these pyrenylpyridines are structurally related, aforementioned properties were found to be quite diverse, particularly in the solid state. These differences stem from factors such as molecular symmetry, extent of inter/intramolecular interactions, and molecular conformations of pyrene units. All pyrenylpyridines exhibited high thermal and photo stability, excellent PLQY values, and electronic properties that are suitable for potential optoelectronic applications. Among these pyrenylpyridines, 2,4,6-TPP was found to display the

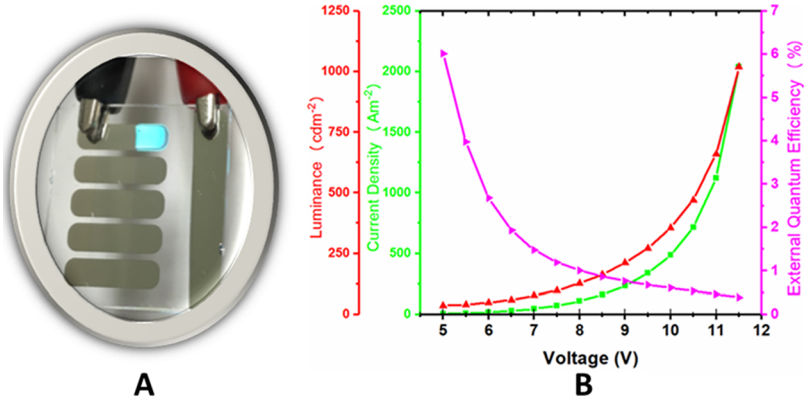

Figure 7. Photograph of electroluminescence from OLED prototype (A) and OLED performance plots (B) with 2,4,6-TPP as the emissive layer.

DOI: 10.1021/acsomega.9b01948
ACS Omega 2019, 4, 16867−16877

highest thermal and photo stability as well as the lowest crystallinity in thin films, as well as the highest PLQY. Therefore, a prototype OLED device was fabricated using 2,4,6-TPP as the nondoped emissive layer. The device showed bright sky-blue electroluminescence and reached a luminance value of 100 cd m^{-2} at 7.5 V, with EQE of 1.2 (±0.1)%, power efficiency of 1.1 (±0.1) Lm W^{-1}, and current efficiency of 1.4 (±0.1) cd A^{-1}. This indicated a good balance of electron and hole transport, and high exciton formation efficiency in 2,4,6-TPP. Evaluation of structure−property relationships of these pyrenylpyridines as model compounds related to pyrene aided understanding of the important role of morphology induced inter- and intramolecular interactions, that are known to tremendously affect the spectral and physical characteristics of structurally similar molecules. Future directions for this research involve fabrication and characterization of OLED prototypes for DPPs and fabrication of more complex OLED devices to further improve the device performance.

EXPERIMENTAL SECTION

Materials. The compounds, 1-pyrenylboronic acid, 2,4,6-tribromopyridine, 2,4-dibromopyridine, 2,6-dibromopyridine, and 1,3,5-tris(1-phenyl-1*H*-benzimidazole-2-yl)benzene (TPBI, sublimed grade), were purchased from Tokyo Chemical Industries Co. Ltd. (Portland, OR) and 1,4-dioxane was purchased from Acros Organics (West Chester, PA). Tetrakis(triphenylphosphine)palladium(0), tetrabutylammonium hexafluorophosphate ($TBAPF_6$), ferrocene (Fc), and *N*,*N*′-di(1-naphthyl)-*N*,*N*′-diphenyl-(1,1′-biphenyl)-4,4′-diamine (NPB, sublimed grade) were purchased from Sigma-Aldrich (St. Louis, MO), whereas 3,5-dibromopyridine was purchased from Alfa Aesar (Ward Hill, MA). Potassium carbonate (K_2CO_3) was purchased from Fisher Scientific (Fair Lawn, NJ). Analytical grade solvents, chloroform ($CHCl_3$), tetrahydrofuran, hexane, acetone, isopropanol, ethyl acetate (EA), methanol (MeOH), DMSO, acetonitrile (ACN), and dichloromethane (DCM), were purchased from Macron (Center Valley, PA). Aluminum (Al) and calcium (Ca) were purchased from Angstrom Engineering Inc. (99.999%, Kitchener, ON). Indium tin oxide (ITO) coated glass (sheet resistance of 8−12 Ω square^{-1}) was purchased from Delta Technologies (Loveland, Co). Column chromatography was performed using a silica gel (Sorbent Technologies, 60 Å, 40−63 μm) slurry packed into glass columns.

Instrumentation. All UV−vis absorption spectra of compounds were recorded using a scanning spectrophotometer (UV−3101PC, Shimadzu, Columbia, MD) and quartz cuvettes (Starna Cells, Atascadero, CA) with path lengths of 1 cm (for solutions) or quartz slides (for thin films, Ted Pella, Inc., Redding, CA). Photoluminescence spectra were acquired using a HORIBA Spex FluoroLog-3 spectrofluorometer (model FL3-22TAU3, Jobin-Yvon, Edison, NJ), with entrance and exit slit widths maintained at 3 or 5 nm and using quartz cuvettes (Starna Cells, Atascadero, CA) with path lengths of 0.4 or 1 cm or quartz slides (for thin films, Ted Pella, Inc., Redding, CA). The same fluorometer was used for time-dependent kinetic photostability measurements with a 14 nm entrance slit width, as well as for the absolute PLQY experiments, by connecting an integrating sphere to the fluorometer (HORIBA Scientific Quanta φ accessory, model FL3-22TAU3, HORIBA Scientific, Edison, NJ). Fluorescence lifetime experiments based on time-correlated single photon counting were performed using a HORIBA FluoroMax plus fluorometer with a pulsed laser DeltaDiode (375 nm, pulse width 45 ps) and a PPD-850 detector with a transit time spread of 180 ps (Horiba Scientific, Edison, NJ). All CV experiments were performed at room temperature using an Autolab PGSTAT 302 potentiostat (Metrohm, Riverside, FL) with a three-electrode system, that is, a platinum disk working electrode, a $Ag/AgNO_3$ non-aqueous reference electrode, and a Pt wire counter electrode (CH Instruments, Austin, TX). The reference electrode was checked against a ferrocene standard before and after each experiment and measured potentials were reported against the Fc/Fc^+ redox potential value. The scan rate was maintained at 0.1 V s^{-1} within the potential range of −0.5 to +3.0 V and $TBAPF_6$ (in DCM or ACN, 0.1 M) was used as the supporting electrolyte. Thermal stability studies were performed using a Hi Res Modulated TGA 2950 thermogravimetric analyzer (TA Instruments, New Castle, DE). Typically, TGA experiments were conducted by heating samples of pyrenylpyridines (<5 mg) under a nitrogen atmosphere from 25 to 600 °C at a constant rate (10 °C min^{-1}). Because thermal decomposition of organic compounds is typically accompanied by formation of volatile compounds, the temperature at which an onset of weight loss (<5%) occurs is reported as the onset decomposition temperature of the compound (T_{onset}). The T_{onset} values are determined using a step-tangent method derived from TA software. Single-crystal XRD analysis was performed using a Bruker Kappa APEX-II DUO diffractometer (Bruker, Madison, WI). Malvern PANalytical Empyrean multipurpose diffractometer (Westborough, MA) with a copper anode was used for PXRD experiments. Grazing incidence X-ray scattering measurements were performed at beamline 8-ID-E of the Advanced Photon Source at Argonne National Laboratory using an X-ray wavelength of 1.6868 Å.[27] The area detector, a PILATUS 1M pixel array detector (Dectris, Switzerland), was positioned 204 mm from the sample. The sample was measured under vacuum and the scattering measured at two different detector heights using an incident angle of 0.18° and exposure time of 5 s. Combining corresponding images eliminated rows of inactive pixels between detector modules and verified that samples were not damaged by the synchrotron beam. The acquired data (as two-dimensional images) were further treated and analyzed using GIXSGUI software package.[28]

An ultra-high VTE system (Angstrom Engineering, Kitchener, ON) was used for OLED prototype fabrication. These OLED prototypes were fabricated in accordance with state-of-the-art protocols.[2,6,29] In summary, OLED prototypes were fabricated using the following steps. First, ITO-coated glass was ultrasonicated sequentially in detergent solution, deionized (DI) water, acetone, and isopropanol followed by exposure to oxygen plasma under ambient conditions for 20 min. Next, OLED prototypes were fabricated by depositing organic layers on clean ITO coated glass substrates using the VTE system, maintained at a base pressure less than 1×10^{-6} Torr during all depositions. Deposition rates were 0.3 Å s^{-1} (Ca), 1 Å s^{-1} (NPB, 2,4,6-TPP, and TPBI), and 2 Å s^{-1} (Al). Layer thickness calibration was achieved using a Bruker DektakXT surface profilometer (Bruker, Madison, NJ). Electroluminescence spectra and performance characteristics of OLED prototypes were obtained using a PTI QuantaMaster4/2006SE spectrofluorometer (Photon Technology International, Edison, NJ), combined with an integrating sphere (Labsphere, North Sutton, NH). Total spectral flux was calibrated using a SCL-050 lamp standard (Labsphere, North

DOI: 10.1021/acsomega.9b01948
ACS Omega 2019, 4, 16867−16877

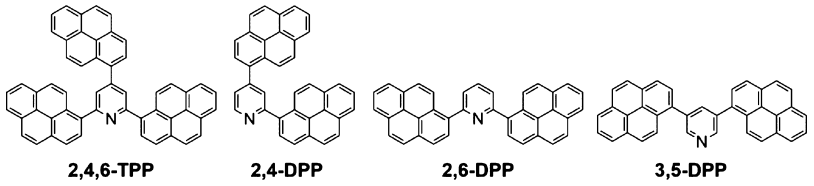

Figure 8. Chemical structures of four pyrenylpyridines prepared in this study.

Sutton, NJ). Current and voltage of OLED prototypes were controlled and measured using a Keithley 2601 source meter (Tektronix, Inc., Beaverton, OR).

Computational Details. DFT computational calculations were performed using hybrid three-parameter non-local exchange functional developed by Becke with Lee–Yang–Parr correlation functional (B3LYP) to obtain energies and geometries of pyrenylpyridines.[30,31] The resolution of the identity (RI) approach was employed for speeding up the computation through effective calculation of the two-electron integrals.[32] These calculations were performed using a triple-zeta valence plus polarization basis set (such as def2-TZVP).[33] Vibrational frequencies confirmed identity of optimized structures at local minima and results were obtained by employing the Turbomole program suite (version 4.2).[34]

Synthesis of Pyrenylpyridines. The four pyrenylpyridine compounds displayed in Figure 8, that is, 2,4-DPP, 2,6-DPP, 3,5-DPP, and 2,4,6-TPP, were synthesized using a one-step Suzuki coupling reaction between respective bromopyridines and 1-pyrenylboronic acid.[35] Synthesis of 2,4,6-TPP is described here as a representative protocol that is applied to the synthesis of all pyrenylpyridines with slight modifications. An Airfree flask was charged with 2,4,6-tribromopyridine (126 mg, 0.40 mmol), 1-pyrenylboronic acid (320 mg, 1.30 mmol), and tetrakis(triphenylphosphine)palladium(0) catalyst (60 mg, 0.05 mmol) inside a glove box. Afterward, 1,4-dioxane (60 mL, degassed for 30 min) and aqueous K_2CO_3 (0.2 M, 15 mL, degassed for 30 min) were added to the flask while purging with argon. The resulting mixture was stirred at 80 °C for 72 h under an argon atmosphere in the sealed flask, followed by chloroform extraction. The combined organic layers were washed several times with brine solution and DI water, and then dried using anhydrous magnesium sulfate. The solvent was removed in vacuo, and the crude product was purified using flash column chromatography on silica gel (eluent hexanes/EA ratio of 9:1 v/v) three times. After solvent evaporation, 2,4,6-TPP was obtained as a light-yellow powder (198 ± 16 mg, yield 73 ± 6%). Further details on DPP synthesis are provided in Supporting Information along with characterization data using ^{13}C NMR, ^{1}H NMR, (Bruker AVANCE 400), and ESI-MS (Agilent 6210 ESI-TOF).

■ ASSOCIATED CONTENT

Supporting Information

The Supporting Information is available free of charge on the ACS Publications website at DOI: 10.1021/acsomega.9b01948.

Single-crystal XRD derived ORTEP diagrams of DPPs; PXRDs of pyrenylpyridines; molecular packing of DPPs in the unit cells derived from single-crystal XRD; calculated (at B3LYP/def2-TZVP level) spatial distribution of frontier molecular orbitals of DPPs; thermogravimetric profiles of pyrenylpyridines; DSC of pyrenylpyridines; time-dependent relative photoluminescence intensity spectra of pyrenylpyridines in dilute chloroform solutions over a period of 1500 s; fluorescence emission maxima (nm) of pyrenylpyridines in different solvents; fluorescence decay curves of pyrenylpyridines solid films monitored at emission maxima with a 1.5 nm band pass and excitation at 375 nm; cyclic voltammograms of pyrenylpyridines in 0.1 M $TBAPF_6$ in CH_2Cl_2 (potential vs Fc/Fc^+); epifluorescence image of 2,4,6-TPP thin film on glass substrate; photoluminescence and electroluminescence (in OLED device) of 2,4,6-TPP in solid state; synthesis of DPPs; characterization of pyrenylpyridines; and HRMS spectra of pyrenylpyridines (PDF)

■ AUTHOR INFORMATION

Corresponding Author

*E-mail: iwarner@lsu.edu. Fax: 1-225-578-3971. Phone: 1-225-578-2829.

ORCID

Frank R. Fronczek: 0000-0001-5544-2779
Evgueni E. Nesterov: 0000-0003-2407-9174
Isiah M. Warner: 0000-0002-5336-7653

Present Addresses

[§]Department of Chemistry and Biochemistry, Northern Illinois University, DeKalb, Illinois 60115, USA.
[∥]YTC America Inc., 3401 Calle Tecate, Camarillo, California 93012, USA.
[⊥]Centre for Advanced Particle Processing and Transport, Newcastle Institute for Energy and Resources, The University of Newcastle, Callaghan, NSW 2308, Australia.
[#]Department of Chemistry, Vanderbilt University, Nashville, Tennessee 37235, USA.
[¶]Department of Chemistry, Indian Institute of Technology Delhi, Delhi 110016, India.

Author Contributions

This manuscript was written through contributions of all authors. All authors have given approval to the final version of the manuscript.

Notes

The authors declare no competing financial interest.

■ ACKNOWLEDGMENTS

The authors gratefully acknowledge financial support through NASA cooperative agreement NNX 16AQ93A under contract number NASA/LEQSF (2016-19)-Phase 3-10; the Louisiana State University Leveraging Innovation for Technology Transfer ($LIFT^2$) grant under number LSU-2018-LIFT-007; and the National Science Foundation under grant no. CHE-1508726. Any opinions, findings, and conclusions or recommendations expressed in this material are those of the author(s) and do not necessarily reflect the views of the National Science Foundation. Authors acknowledge Dr. Sourav Chatterjee (University of Delaware), Dr. Xiaochu Wu

DOI: 10.1021/acsomega.9b01948
ACS Omega 2019, 4, 16867−16877

(Shared Instrument Facility, LSU), Dr. Rafael Cueto (Polymer Analysis Lab, LSU) and Wanda S. LeBlanc (Shared Instrument Facility, LSU) for assistance with GIWAXS, fluorescence imaging, TGA and PXRD experiments. Finally, the authors gratefully acknowledge Dr. Caitlan E. Ayala for editorial comments regarding this manuscript.

REFERENCES

(1) Gupta, A. S. *Organic Light Emitting Diodes (OLEDs): Technologies and Global Markets*; BCC Research: Massachusetts, 2015; pp 7−14, 90−120.
(2) Martens, R. *The OLED Handbook: A Guide to OLED Technology, Industry & Market*; LULU Press: North Carolina, 2014; pp 11−36.
(3) Zhu, M.; Yang, C. Blue fluorescent emitters: Design tactics and applications in organic light-emitting diodes. *Chem. Soc. Rev.* **2013**, *42*, 4963−4976.
(4) Yang, X.; Xu, X.; Zhou, G. Recent advances of the emitters for high performance deep-blue organic light-emitting diodes. *J. Mater. Chem. C* **2015**, *3*, 913−944.
(5) Salunke, J. K.; Sonar, P.; Wong, F. L.; Roy, V. A.; Lee, C. S.; Wadgaonkar, P. P. Pyrene based conjugated materials: synthesis, characterization and electroluminescent properties. *Phys. Chem. Chem. Phys.* **2014**, *16*, 23320−23328.
(6) Su, W. Printed organic light emission and display. In *Printed Electronics*; Cui, Z., Ed.; John Wiley & Sons: New York, 2016; pp 251−260.
(7) Hu, J.-Y.; Yamato, T. Synthesis and photophysical properties of pyrene-based multiply conjugated shaped light-emitting architectures: Toward efficient organic-light-emitting diodes. In *Organic Light Emitting Diode—Material, Process and Devices*; Ko, S. H., Ed.; InTech: Croatia, 2011; pp 22−54.
(8) Amarnath, C. A.; Kim, H. K.; Yi, D. K.; Lee, S.; Do, Y. R.; Paik, U. Novel electroluminescent polymer derived from pyrene-functionalized polyaniline. *Bull. Korean Chem. Soc.* **2011**, *32*, 1495−1499.
(9) Sonar, P.; Soh, M. S.; Cheng, Y. H.; Henssler, J. T.; Sellinger, A. 1,3,6,8-tetrasubstituted pyrenes: solution-processable materials for application in organic electronics. *Org. Lett.* **2010**, *12*, 3292−3295.
(10) Okinara, K.; Yamada, N.; Igawa, S.; Kamatani, J.; Yashima, M. Organic light-emitting device. WIPO Patent WO2007072741A1, June 28, 2007.
(11) Yang, C.-H.; Guo, T.-F.; Sun, I.-W. Highly efficient greenish blue-emitting organic diodes based on pyrene derivatives. *J. Lumin.* **2007**, *124*, 93−98.
(12) Chercka, D.; Yoo, S.-J.; Baumgarten, M.; Kim, J.-J.; Mullen, K. Pyrene based materials for exceptionally deep blue OLEDs. *J. Mater. Chem. C* **2014**, *2*, 9083−9086.
(13) Pu, Y.-J.; Yoshizaki, M.; Akiniwa, T.; Nakayama, K.-I.; Kido, J. Dipyrenylpyridines for electron-transporting materials in organic light emitting devices and their structural effect on electron injection from Li/Al cathode. *Org. Electron.* **2009**, *10*, 877−882.
(14) Jeon, W. S.; Hyoung-Yun, O.; Park, J. S.; Kwon, J. H. High Mobility Electron Transport Material with Pyrene Moiety for Organic Light-Emitting Diodes (OLEDs). *Mol. Cryst. Liq. Cryst.* **2011**, *550*, 311−319.
(15) Zhou, Y.; Kim, J. W.; Kim, M. J.; Son, W.-J.; Han, S. J.; Kim, H. N.; Han, S.; Kim, Y.; Lee, C.; Kim, S. J.; Kim, D. H.; Kim, J.-J.; Yoon, J. Novel bi-nuclear boron complex with pyrene ligand: red-light emitting as well as electron transporting material in organic light-emitting diodes. *Org. Lett.* **2010**, *12*, 1272−1275.
(16) Oh, H.; Lee, C.; Lee, S. Efficient blue organic light-emitting diodes using newly-developed pyrene-based electron transport materials. *Org. Electron.* **2009**, *10*, 163−169.
(17) Wu, K.-C.; Ku, P.-J.; Lin, C.-S.; Shih, H.-T.; Wu, F.-I.; Huang, M.-J.; Lin, J.-J.; Chen, I.-C.; Cheng, C.-H. The photophysical properties of dipyrenylbenzenes and their application as exceedingly efficient blue emitters for electroluminescent devices. *Adv. Funct. Mater.* **2008**, *18*, 67−75.
(18) Keawin, T.; Prachumrak, N.; Namuangruk, S.; Pansay, S.; Kungwan, N.; Maensiri, S.; Jungsuttiwong, S.; Sudyoadsuk, T.; Promarak, V. Efficient bifunctional materials based on pyrene- and triphenylamine-functionalized dendrimers for electroluminescent devices. *RSC Adv.* **2015**, *5*, 73481−73489.
(19) Yuan, W. Z.; Lu, P.; Chen, S.; Lam, J. W.; Wang, Z.; Liu, Y.; Tang, B. Z. Changing the behavior of chromophores from aggregation-caused quenching to aggregation-induced emission: development of highly efficient light emitters in the solid state. *Adv. Matter* **2010**, *22*, 2159−2163.
(20) Chan, K. L.; Lim, J. P. F.; Yang, X.; Dodabalapur, A.; Jabbour, G. E.; Sellinger, A. High-efficiency pyrene-based blue light emitting diodes: aggregation suppression using a calixarene 3D-scaffold. *Chem. Commun.* **2012**, *48*, 5106−5108.
(21) Lakovicz, J. R. *Principles of Fluorescence Spectroscopy*; Springer: New York, 2006; pp 9−12, 103−124.
(22) Zhao, Z.; Chen, S.; Lam, J. W. Y.; Wang, Z.; Lu, P.; Mahtab, F.; Sung, H. H. Y.; Williams, I. D.; Ma, Y.; Kwok, H. S.; Tang, B. Z. Pyrene-substituted ethenes: aggregation-enhanced excimer emission and highly efficient electroluminescence. *J. Mater. Chem.* **2011**, *21*, 7210−7216.
(23) Zhang, Y.; He, B.; Liu, J.; Hu, S.; Pan, L.; Zhao, Z.; Tang, B. Z. Aggregation-induced emission and the working mechanism of 1-benzoyl and 1-benzyl pyrene derivatives. *Phys. Chem. Chem. Phys.* **2018**, *20*, 9922−9929.
(24) Lo, M. Y.; Zhen, C.; Lauters, M.; Jabbour, G. E.; Sellinger, A. Organic−Inorganic Hybrids Based on Pyrene Functionalized Octavinylsilsesquioxane Cores for Application in OLEDs. *J. Am. Chem. Soc.* **2007**, *129*, 5808−5809.
(25) Lee, E.-Y.; Hwang, S.-H.; Kim, Y.-K.; Jung, H.-J.; Park, J.-H.; Lim, J.-O.; Han, S.-H.; Jeong, E.-J.; Kim, S.-Y.; Lee, J.-H. Condensed cyclic compound and organic light-emitting device comprising the same. U.S. Patent 20,140,183,463A1, July 3, 2014.
(26) Cho, S.-J.; Lee, C.-M. Condensed cyclic compound and organic light-emitting device including the same. U.S. Patent 20,150,263,290A1, Sept 17, 2015.
(27) Jiang, Z.; Li, X.; Strzalka, J.; Sprung, M.; Sun, T.; Sandy, A. R.; Narayanan, S.; Lee, D. R.; Wang, J. The dedicated high-resolution grazing-incidence X-ray scattering beamline 8-ID-E at the Advanced Photon Source. *J. Synchrotron Radiat.* **2012**, *19*, 627−636.
(28) Jiang, Z. GIXSGUI: a MATLAB toolbox for grazing-incidence X-ray scattering data visualization and reduction, and indexing of buried three-dimensional periodic nanostructured films. *J. Appl. Crystallogr.* **2015**, *48*, 917−926.
(29) Koden, M. *OLED Displays and Lighting*; John Wiley & Sons: New York, 2017; pp 12−24, 103−116.
(30) Burke, K.; Perdew, J. P.; Wang, Y. In *Electronic Density Functional Theory: Recent Progress and New Directions*; Dobson, J. F., Vignale, G., Das, M. P., Eds.; Plenum Publishers; New York, 1998; pp 81−113.
(31) Becke, A. D. Density-functional thermochemistry. III. The role of exact exchange. *J. Chem. Phys.* **1993**, *98*, 5648−5652.
(32) Hättig, C. Geometry optimizations with the coupled-cluster model CC2 using the resolution-of-the-identity approximation. *J. Chem. Phys.* **2003**, *118*, 7751−7761.
(33) Weigend, F.; Ahlrichs, R. Balanced basis sets of split valence, triple zeta valence and quadruple zeta valence quality for H to Rn: Design and assessment of accuracy. *Phys. Chem. Chem. Phys.* **2005**, *7*, 3297−3305.
(34) Ahlrichs, R.; Bär, M.; Häser, M.; Horn, H.; Kölmel, C. Electronic structure calculations on workstation computers: the program system turbomole. *Chem. Phys. Lett.* **1989**, *162*, 165−169.
(35) Miyaura, N.; Suzuki, A. Palladium-catalyzed cross-coupling reactions of organoboron compounds. *Chem. Rev.* **1995**, *95*, 2457−2483.
(36) Müller-Buschbaum, P. The active layer morphology of organic solar cells probed with grazing incidence scattering techniques. *Adv. Mater.* **2014**, *26*, 7692−7709.

DOI: 10.1021/acsomega.9b01948
ACS Omega 2019, 4, 16867−16877

(37) Moorthy, J. N.; Venkatakrishnan, P.; Natarajan, P.; Huang, D.-F.; Chow, T. J. De Novo Design for Functional Amorphous Materials: Synthesis and Thermal and Light-Emitting Properties ofTwistedAnthracene-Functionalized Bimesitylenes. *J. Am. Chem. Soc.* **2008**, *130*, 17320−17333.
(38) Kwak, K.; Cho, K.; Kim, S. Analysis of thermal degradation of organic light-emitting diodes with infrared imaging and impedance spectroscopy. *Opt. Express* **2013**, *21*, 29558−29566.
(39) Kaya, İ.; Aydın, A. Synthesis and characterization of the polyaminophenol derivatives containing thiophene in side chain: Thermal degradation, electrical conductivity, optical-electrochemical, and fluorescent properties. *J. Appl. Polym. Sci.* **2011**, *121*, 3028−3040.
(40) Eshetu, G. G.; Jeong, S.; Pandard, P.; Lecocq, A.; Marlair, G.; Passerini, S. Comprehensive insights into the thermal stability, biodegradability, and combustion chemistry of pyrrolidinium-based ionic liquids. *ChemSusChem* **2017**, *10*, 3146−3159.
(41) Kondakov, D. Y. In *OLED Fundamentals: Materials, Devices, and Processing of Organic Light-Emitting Diodes*; Gaspar, D. J., Polikarpov, E., Eds.; CRC Press: FL, 2015; pp 339−365.
(42) Vogelsang, J.; Kasper, R.; Steinhauer, C.; Person, B.; Heilemann, M.; Sauer, M.; Tinnefeld, P. A Reducing and Oxidizing System Minimizes Photobleaching and Blinking of Fluorescent Dyes. *Angew. Chem., Int. Ed.* **2008**, *47*, 5465−5469.
(43) Hoogenboom, J. P.; van Dijk, E. M.; Hernando, J.; van Hulst, N. F.; Garcia-Parajo, M. F. Power-law-distributed dark states are the main pathway for photobleaching of single organic molecules. *Phys. Rev. Lett.* **2005**, *95*, 097401.
(44) Neumüller, K. G.; Elsayad, K.; Reisecker, J. M.; Waxham, M. N.; Heinze, K. G. Photounbinding of calmodulin from a family of CaM binding peptides. *PLoS One* **2010**, *5*, No. e14050.
(45) Siraj, N.; Hasan, F.; Das, S.; Kiruri, L. W.; Steege Gall, K. E.; Baker, G. A.; Warner, I. M. Carbazole-derived group of uniform materials based on organic salts: solid state fluorescent analogues of ionic liquids for potential applications in organic-based blue light-emitting diodes. *J. Phys. Chem. C* **2014**, *118*, 2312−2320.
(46) De Silva, T. P. D.; Sahasrabudhe, G.; Yang, B.; Wang, C.-H.; Chhotaray, P. K.; Nesterov, E. E.; Warner, I. M. Influence of anion variations on morphological, spectral, and physical properties of the propidium luminophore. *J. Phys. Chem. A* **2019**, *123*, 111.
(47) Kolic, P. E.; Siraj, N.; Hamdan, S.; Regmi, B. P.; Warner, I. M. Synthesis and characterization of porphyrin-based GUMBOS and nanoGUMBOS as improved photosensitizers. *J. Phys. Chem. C* **2016**, *120*, 5155−5163.
(48) Valeur, B. *Molecular Fluorescence: Principles and Applications*; Wiley-VCH Verlag GmbH: Weinheim, 2001; pp 92−98.
(49) Song, H.-Z.; Bao, X.-M.; Li, N.-S.; Zhang, J.-Y. Relation between electroluminescence and photoluminescence of Si+-implanted SiO2. *J. Appl. Phys.* **1997**, *82*, 4028.
(50) Anderson, M. R.; Yu, G.; Heeger, A. J. Photoluminescence and electroluminescence of films from soluble PPV-polymers. *Synth. Met.* **1997**, *85*, 1275−1276.
(51) Würth, C.; Grabolle, M.; Pauli, J.; Spieles, M.; Resch-Genger, U. Relative and absolute determination of fluorescence quantum yields of transparent samples. *Nat. Protoc.* **2013**, *8*, 1535−1550.
(52) Strehlow, W. H.; Cook, E. L. Compilation of energy band gaps in elemental and binary compound semiconductors and insulators. *J. Phys. Chem. Ref. Data* **1973**, *2*, 163−200.
(53) Bard, A. J.; Faulkner, L. R. *Electrochemical Methods Fundamentals and Applications*; John Wiley & Sons: New York, USA, 2001; pp 156−261.
(54) Zhou, Y.; He, Q.; Yang, Y.; Zhong, H.; He, C.; Sang, G.; Liu, W.; Yang, C.; Bai, F.; Li, Y. Binaphthyl-Containing Green- and Red-Emitting Molecules for Solution-Processable Organic Light-Emitting Diodes. *Adv. Funct. Mater.* **2008**, *18*, 3299−3306.
(55) Cardona, C. M.; Li, W.; Kaifer, A. E.; Stockdale, D.; Bazan, G. C. Electrochemical considerations for determining absolute frontier orbital energy levels of conjugated polymers for solar Cell applications. *Adv. Mater.* **2011**, *23*, 2367−2371.
(56) Forrest, S. R.; Bradley, D. D. C.; Thompson, M. E. Measuring the efficiency of organic light-emitting devices. *Adv. Mater.* **2003**, *15*, 1043−1048.
(57) Reineke, S.; Lindner, F.; Schwartz, G.; Seidler, N.; Walzer, K.; Lüssem, B.; Leo, K. White organic light-emitting diodes with fluorescent tube efficiency. *Nature* **2009**, *459*, 234−238.
(58) https://www.oled-info.com/udc-our-rgb1b2-amoled-architecture-minimizes-blue-light-hazard (accessed Feb 24, 2019).
(59) Hack, M.; Brown, J. J.; Weaver, M. S.; D'Andrade, B. OLED Display Architecture. U.S. Patent 9,385,167B2, July 5, 2016.
(60) https://www.oled-info.com/udc-show-new-light-blue-emitter-that-can-be-used-white-oleds-or-four-sub-pixel-displays (accessed Feb 4, 2019).

DOI: 10.1021/acsomega.9b01948
ACS Omega 2019, 4, 16867−16877